Structural model of the open–closed–inactivated cycle of prokaryotic voltage-gated sodium channels

Claire Bagnéris, Claire E. Naylor, Emily C. McCusker, and B.A. Wallace

Institute of Structural and Molecular Biology, Birkbeck College, University of London, London WC1E 7HX, England, UK

In excitable cells, the initiation of the action potential results from the opening of voltage-gated sodium channels. These channels undergo a series of conformational changes between open, closed, and inactivated states. Many models have been proposed for the structural transitions that result in these different functional states. Here, we compare the crystal structures of prokaryotic sodium channels captured in the different conformational forms and use them as the basis for examining molecular models for the activation, slow inactivation, and recovery processes. We compare structural similarities and differences in the pore domains, specifically in the transmembrane helices, the constrictions within the pore cavity, the activation gate at the cytoplasmic end of the last transmembrane helix, the C-terminal domain, and the selectivity filter. We discuss the observed differences in the context of previous models for opening, closing, and inactivation, and present a new structure-based model for the functional transitions. Our proposed prokaryotic channel activation mechanism is then compared with the activation transition in eukaryotic sodium channels.

The Journal of General Physiology

Eukaryotic sodium channels are complex, multidomain proteins that assemble into pseudotetrameric structures. Sodium channels are also present in some prokaryotes (Ren et al., 2001), where they are homologous but simpler, single-domain proteins that assemble to form functional homotetramers (Nurani et al., 2008). Both eukaryotic and prokaryotic sodium channels consist of voltage-sensor (VS) and pore regions that are physically separated in three dimensions. Pore-only channels can be constructed, which are capable of undergoing opening and closing transitions and support ion flux in a manner similar to that of intact channels (McCusker et al., 2011; Shaya et al., 2011). Although the kinetics of their processes of conversion between states are different, both eukaryotic and prokaryotic channels exhibit activation, recovery, and slow inactivation transitions (Koishi et al., 2004; Charalambous and Wallace, 2011); in addition, eukaryotic channels undergo a fast inactivation process that is not observed in prokaryotic channels (Pavlov et al., 2005). Prokaryotic sodium channels have also been shown to be blocked by eukaryotic sodium channel antagonists (Bagnéris et al., 2014).

Many models have been proposed for the structural changes that result in the open, closed, and slow inactivated states of prokaryotic sodium channels (e.g., Kuzmenkin et al., 2004; Zhao et al., 2004; Pavlov et al., 2005; Shafrir et al., 2008). Although there are, as yet, no crystal structures of eukaryotic sodium channels, the structures of several prokaryotic sodium channel orthologues have recently been determined by x-ray crystallography (Payandeh et al., 2011, 2012; McCusker et al., 2012; Zhang et al., 2012; Bagnéris et al., 2013; Shaya et al., 2014). These include the voltage-gated sodium channels from *Magnetococcus marinus*, formerly known as *Magnetococcus spirillium* (NavMs); from *Arcobacter butzler* (NavAb); from *Rickettsiales sp. HIMB114* (NavRh); and from *Alkalilimnicola ehrlichei* (NavAe). These structures now make it possible to observe various states of prokaryotic sodium channels because they have apparently captured the pore regions in partially and fully open (NavMs), closed (NavAb and NavAe), and inactivated (NavAb and NavRh) conformations, thereby enabling structural comparisons that provide new insights into the transition processes.

Because the transmembrane pore regions of the NavMs and NavAb pores have very high sequence identities (~69%; McCusker et al., 2012; Fig. 1), our comparisons will primarily be confined to these structures because with this level of similarity, differences seen are likely to be state dependent rather than a consequence of sequence dissimilarities. They enable comparisons of structures that we designate as the following: partially ($pOpen_{Ms}$; Protein Data Bank [PDB] accession no. 4F4L; 3.5-Å resolution; McCusker et al., 2012) and fully open ($Open_{Ms}$; PDB accession no. 3ZJZ, 2.9-Å resolution; Bagnéris et al., 2013), closed ($Closed_{Ab}$; PBD accession no. 3RVY, an I217C mutant; 2.7-Å resolution;

Correspondence to B.A. Wallace: b.wallace@mail.cryst.bbk.ac.uk

E.C. McCusker's present address is Teva Pharmaceuticals, Chicago, IL 60622

Abbreviations used in this paper: CTD, C-terminal domain; NavAb, voltage-gated sodium channel from *Arcobacter butzleri*; NavAe, voltage-gated sodium channel from *Alkalilimnicola ehrlichei*; NavMs, voltage-gated sodium channel from *Magnetococcus marinus*; NavRh, voltage-gated sodium channel from *Rickettsiales sp. HIMB114*; SF, selectivity filter; VS, voltage sensor.

The Rockefeller University Press
J. Gen. Physiol. Vol. 145 No. 1 5–16
www.jgp.org/cgi/doi/10.1085/jgp.201411242

Payandeh et al., 2011), and inactivated ($Inactivated_{Ab}$; PDB accession no. 4EKW, 3.2-Å resolution; Payandeh et al., 2012) forms. The other inactivated form for which there is a crystal structure, NavRh (PDB accession no. 4DXW; 3.0-Å resolution; Zhang et al., 2012), and the other closed form, NavAe (PDB accession no. 4LTO; 3.5-Å resolution; Shaya et al., 2014), are more distant homologues (only 42 and 45% identity, respectively, in the pore region; Fig. 1). In addition, although both the NavAb and NavMs homologues have been shown to support sodium flux (Payandeh et al., 2011; D'Avanzo et al., 2013), neither NavRh nor NavAe has yet been shown to exhibit functional activity; therefore, we considered them to be less suitable for detailed comparisons. Although the resolutions of the structures are modest, all are sufficient to define the types and magnitudes of the conformational differences described in the comparisons made in this Review. In addition to these crystal structures, however, two structures of another orthologue, NavCt (PDB accession no. 4BGN, ∼9-Å resolution; Tsai et al., 2013), have been determined by electron crystallography, but those structures are at too low a resolution to make viable comparisons.

This Review focuses on comparisons of the $Closed_{Ab}$–$pOpen_{Ms}$–$Open_{Ms}$–$Inactivated_{Ab}$ crystal structures, developing a structure-based model for the functional transitions. Although these crystal structures provide an important new structural context for understanding the nature of the transitions, it must be remembered that any models developed from them will ultimately require

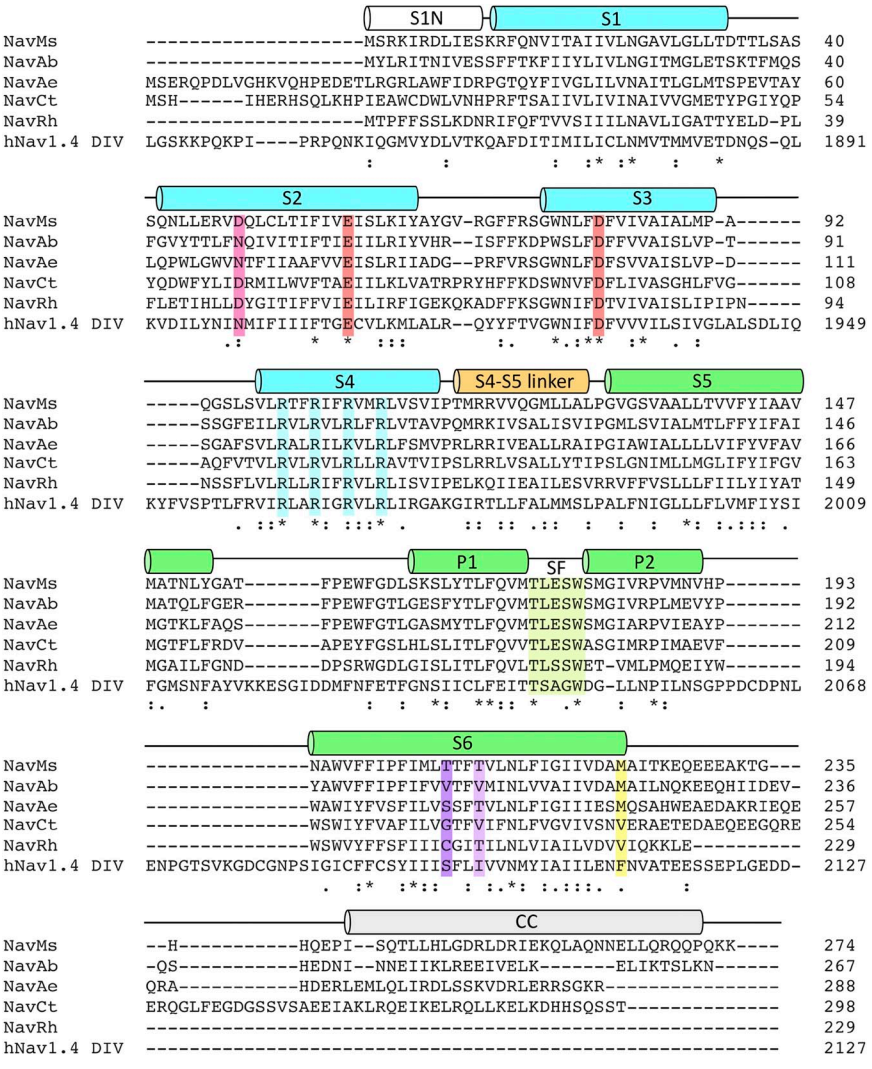

Figure 1. Sequence alignment, using Clustal Omega (Sievers et al., 2011), of the prokaryotic sodium channel orthologues: NavMs from *Magnetococcus marinus* MC-1 (UniProt accession no. A0L5S6), NavAb from *Arcobacter butzleri* RM4018 (UniProt accession no. A8EVM5), NavAe from *Alkalilimnicola ehrlichii* MLHE-1 (UniProt accession no. Q0ABW0), NavCt from *Caldalkalibacillus thermarum* TA2.A1 (UniProt accession no. F5L478), NavRh from *Rickettsiales sp. HIMB114* (UniProt accession no. D0RMU8), and domain IV (DIV) of the human Nav1.4 sodium channel (UniProt accession no. P35499). The identities of the helical regions (transmembrane helices S1–S6), the N-terminal intracellular helix S1N, the S4–S5 linker helix, the P1 and P2 pore helices, and the intracellular C-terminal coiled-coil (CC) helix are indicated in the horizontal colored tubes above the sequences and are based on the crystal structures of NavAb for the VS region (cyan), on the crystal structure of NavMs for the pore region (green), and on the site-directed electron paramagnetic resonance spectroscopy of NavMs and circular dichroism truncation studies of NaChBac for the CTD (gray). The vertical magenta bar indicates the extracellular negatively charged (ENC) region formed by D49 (in S2), and the red bars are the intracellular negatively charged (INC) region formed by E59 (in S2) and D81 (in S3) involved in the gating charge transfer across the membrane through sequential interactions with four arginine residues in S4 (indicated by the cyan vertical bars); in the "up" conformation, which corresponds to the activated state, residues E59 and D81 form the salt-bridged pairs. The residues comprising the SF are highlighted in light green vertical bars. The residues in purple are proposed to be the start of the twist in S6 that is implicated in activation gate opening (light purple from the partially open structure and dark purple in the fully open structure). The residue in yellow indicates the location of the final hydrophobic constriction region (HC3) in the closed structure, which effectively corresponds to the location of the activation gate.

verification by functional studies under voltage-clamp conditions that probe native structures in real time and in the context of cell membranes.

Defining the conformational states represented in the crystal structures

The full-length NavAb channel has its VS in the "up" conformation (with residues E59 and D81 forming salt-bridged pairs to arginines in S4; Fig. 1) (Payandeh et al., 2011). This conformation of the VS is considered to be associated with the activated or fully open state as defined by disulfide cross-linking experiments (DeCaen et al., 2008, 2009). In addition, because in crystals there is no transmembrane potential, we expected that the structure would include an open form of the pore, as would be seen when the channel gate opens in response to membrane depolarization. However, in these crystals, the activation gate, and thus the pore region, appears to be in the closed conformation: the pore has no continuous transmembrane pathway that would enable the passage of sodium ions from the extracellular to the intracellular surface (McCusker et al., 2012; Fig. 2, A and B). Although the selectivity filter (SF) is sufficiently open to enable ions to enter the pore, the bottom of its cavity (at the activation gate) is blocked (Payandeh et al., 2011) so ions cannot exit. This structure has thus been described as being in a "pre-open" state, in other words, with a VS conformation that has primed the gate for opening but in which the gate is actually closed. This demonstrates that the structures of the VS and pore regions can be uncoupled, and may indicate the presence of an additional conformation intermediate between the "open" and "closed" states. In the comparisons in this Review, which focuses on the pore region responsible for the opening and closing of the transmembrane pathway, we have designated this structure as "closed"

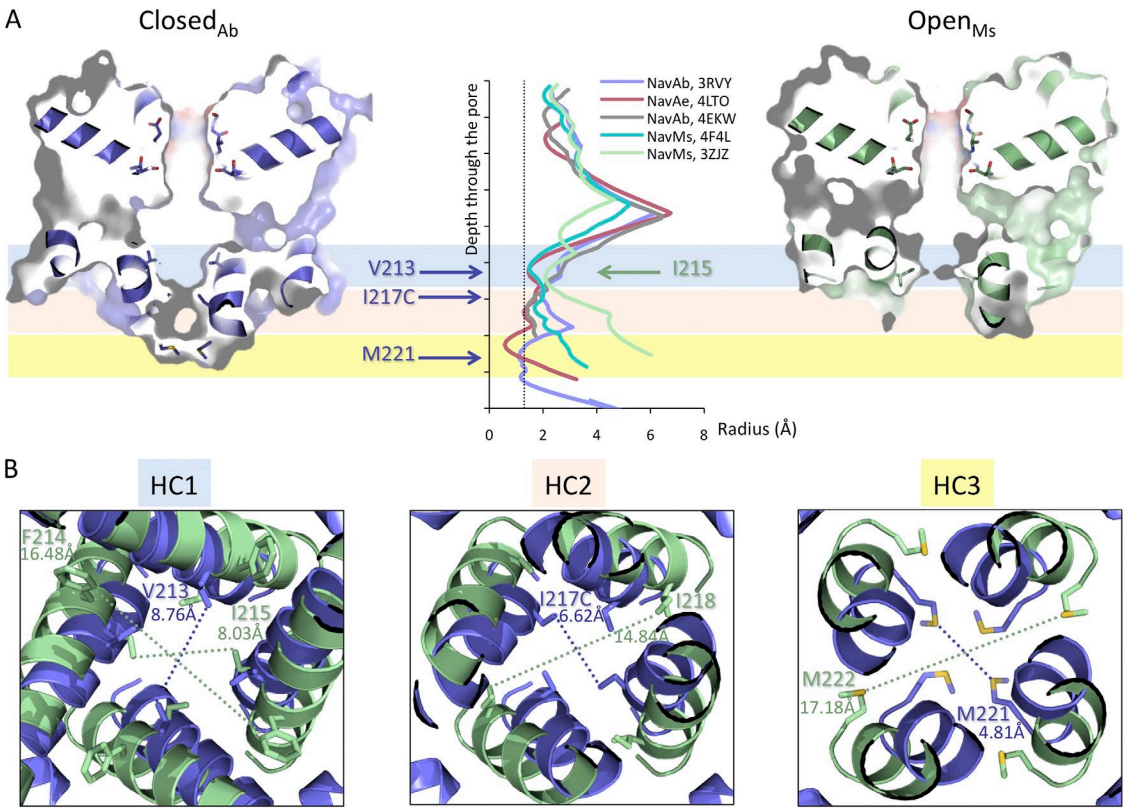

Figure 2. Accessible surface differences between the open and closed structures. (A; middle) Accessible surface plots (made using CAVER software; Chovancova et al., 2012) showing radius versus distance through the central axis of the pore for Closed$_{Ab}$-I217C (slate blue), Closed$_{Ae}$ (red), Inactivated$_{Ab}$ (gray), Open$_{Ms}$ (light green), and pOpen$_{Ms}$ (turquoise). (Left and right) Slab surface mode/cartoon depictions of the pores, sliced along the transmembrane direction for the Closed$_{Ab}$ (left, slate blue) and Open$_{Ms}$ (right, light green) pores, highlighting the sites of the first minor constriction (blue underlay: present for both forms with the responsible residues, V213 in the closed form and I215 in the open form), the second minor construction (orange underlay: present only in the closed form, residue I217C), and the third major constriction (yellow underlay: present only for the closed form, residue M221) at the intracellular end of the cavity. I217C is the mutation in the closed structure that enabled crystallization at higher resolution. (B) Detailed view of the three "hydrophobic constriction" (HC) regions noted above shown in cartoon and stick mode for the Closed$_{Ab}$ (slated blue) and Open$_{Ms}$ (light green) structures. The distances shown were measured between two diagonally opposite residues. It is clear that the narrow constrictions at HC2 and HC3 (6.62 and 4.81 Å) seen in the closed structure are not present in the open structure (where the equivalent distances are 14.84 and 17.18 Å).

($Closed_{Ab}$) based on the state of the pore region. It is very similar in dimensions and features to the NavAe closed pore (Shaya et al., 2014), a structure that does not contain a VS region, another indication that the pore region state is not solely determined by the VS state.

One of the two NavMs pore structures (Bagnéris et al., 2013) has been designated to be in the fully open state ($Open_{Ms}$) by virtue of its transmembrane pathway being of sufficient diameter along the full length of the pore, from the extracellular surface to the intracellular surface (Fig. 2, A and B), to enable the translocation of sodium ions across the cell membrane (Ulmschneider et al., 2013). It has all four monomers with a splayed conformation at their intracellular ends. In contrast, in the partially open ($pOpen_{Ms}$) structure (McCusker et al., 2012) (which lacks the last 37 residues of its C-terminal domain [CTD]), only one of the four monomers of the tetramer adopts an open splayed conformation, with the result that the activation gate is only partially open; it is not sufficient to permit ion translocation but is more widely open than the closed structure (Fig. 2 A). The other three monomers in this structure are effectively

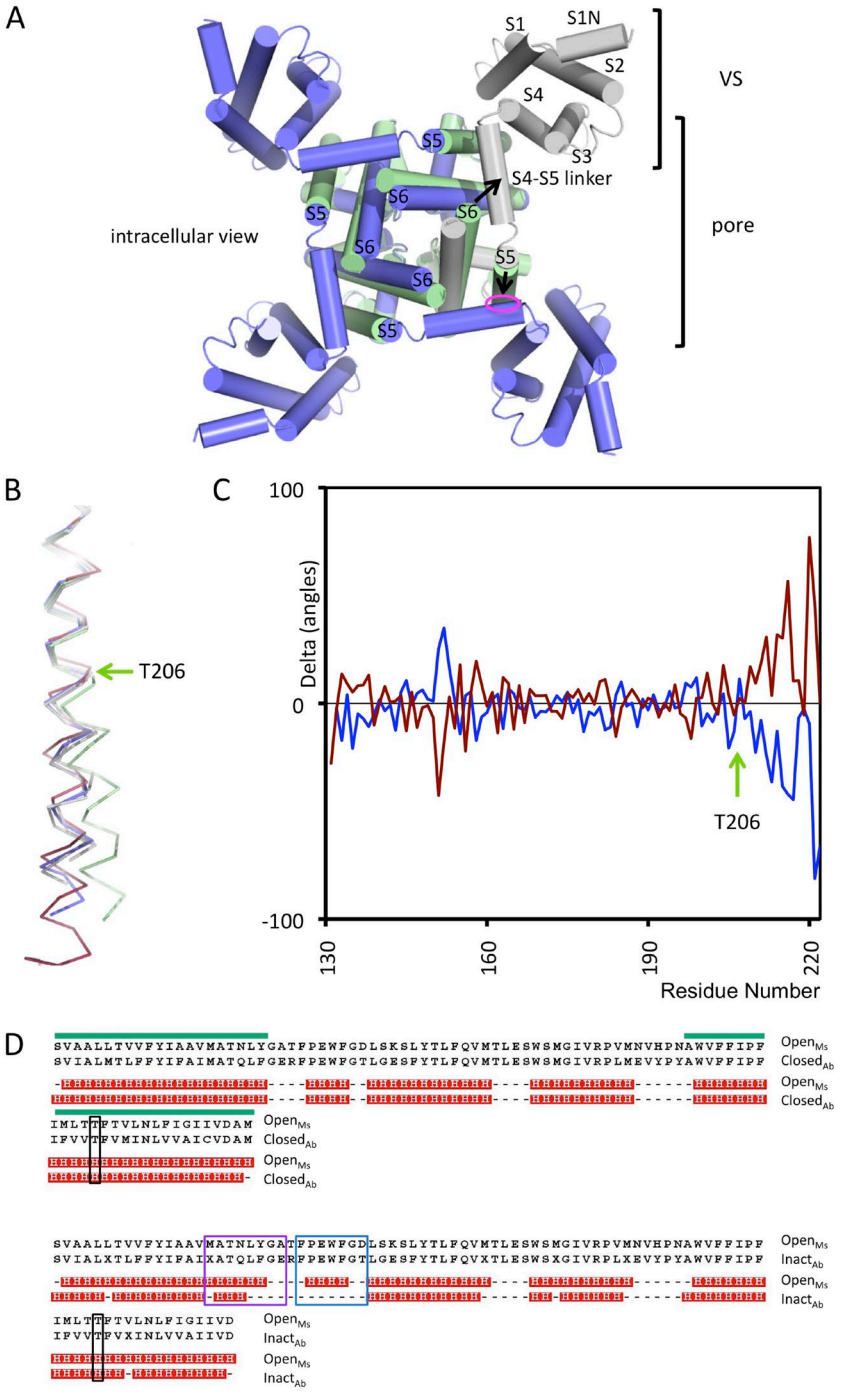

Figure 3. Differences between the open and closed structures. (A) Comparison of the $Open_{Ms}$ (green) pore and the $Closed_{Ab}$ (slate blue) crystal structures, depicted in cylindrical mode viewed from the intracellular surface. The equivalent residue numbers for the pore domain were G129 to M221 in NavMs and G130 to M222 in NavAb. Three-dimensional alignments (in all cases the least-squares superpositions were done using residues 145–198 [or their sequence equivalents] at the top of helices S5 and S6) and figures were made using PyMOL software (Schrödinger, LLC). The motions associated with the S5 and S6 helices are indicated by the small and large arrows, respectively. One of the $Closed_{Ab}$ monomers is shown in gray, so that it can be seen that the region of the S4–S5 linker that the S5 helix in the open state would impinge on (magenta circle) is in the adjacent, not the same, monomer. (B) The Cα carbons of the S6 helixes (in stick motif) showing that the $Closed_{Ab}$ (slate blue), $Inactivated_{Ab}$ (gray), and $Closed_{Ae}$ (red) structures overlay closely, but that the $Open_{Ms}$ (green) deviates from the other structures starting at residue T206. (C) Plot of the delta phi (blue) and delta psi (red) angles in the S6 helix as a function of residue number. Values are those of $Open_{Ms}$ structure (PDB accession no. 3ZJZ-A chain) minus those of the $Closed_{Ab}$ structure (3RVY-A chain), demonstrating that the differences start after residue T206 in NavMs and continue to the end of the S6 helix. The single peak at around residue 155 is not related to the transition but simply arises from different interactions of the two proteins, with the different crystallization detergent molecules present adjacent to this site. (D) Secondary structure alignments compared using the 2Struc server (Klose et al., 2010). The position corresponding to the T206 residue in helix S6 is indicated by the black box in both parts. (Top) $Open_{Ms}$ versus $Closed_{Ab}$. The locations of the S5 and S6 helices are indicated by the horizontal green bars. Both structures have essentially identical secondary structures, even around T206. (Bottom) $Open_{Ms}$ versus $Inactivated_{Ab}$. The biggest differences are at the top of S5 (purple box) and in the turret loop (cyan box), not in helix S6 nor the region around T206.

equivalent to the closed-state pore conformations. A model "open" structure was constructed (McCusker et al., 2012) based on using the most open of the four monomers to produce a symmetric tetramer, which was very similar to the structure later determined of the fully open state (Bagnéris et al., 2013). In the partially open structure, the distal end of the CTD, which has been proposed to form a stabilizing four-helix coiled-coil (Powl et al., 2010; Irie et al., 2012; Bagnéris et al., 2013; Shaya et al., 2014), is absent, although it is present in the fully open structure; this may have enabled the uncoupled opening of the four S6 helices, and this asymmetry suggests there may be an asynchrony in the functional transition between states.

The two inactivated forms of NavAb (Inactivated$_{Ab}$; Payandeh et al., 2012) and NavRh (Inactivated$_{Rh}$; Zhang et al., 2012) have been so designated based on their closed pores and collapsed SFs (although the authors of the NavAb structure were careful to describe it as being in a "potentially" inactivated state, largely because there was no confirming functional data). Both of these structures have closed activation gates, which are very similar to the Closed$_{Ab}$ structure, but their SFs are unlike any of the other structures, and would be too narrow to enable ions to enter the pore (Figs. 2 A, middle, and 4, C and D, and Table S1).

Structural transitions associated with opening and closing

The extracellular turret and vestibule surfaces (comprised of the S5–S6 linker, including the P1, P2, and SF regions; Fig. 1) are very similar in the Open$_{Ms}$ and Closed$_{Ab}$ pores, suggesting that these are not substantially involved in the gating transition. In addition, the N-terminal ends of their S6 helices (Fig. 3 B) are virtually superimposable, as are the C-terminal ends of the S5 helices. However, the intracellular surface features differ substantially (Fig. 3 A) as a result of differences in the relative orientations and splaying of the C-terminal

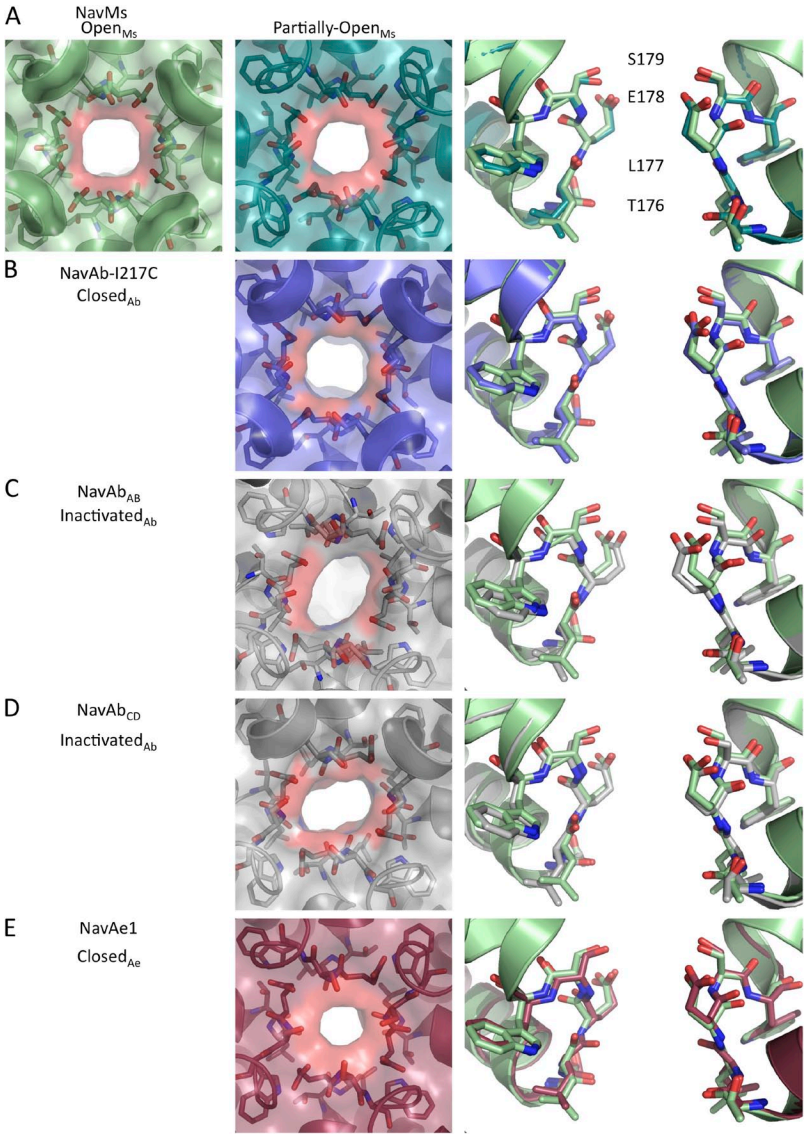

Figure 4. Comparisons of the SF regions. (Left and middle columns) Views from the extracellular surface showing the size of the SF central holes, defined as the white areas in the middle of each structure. (Right column) Side view superpositions of the SFs in cartoon and stick depictions, in each case comparing the Open$_{Ms}$ structure (light green) with the corresponding structure in that row. The identities of the SF residues (TLES) are indicated. Only two monomers are shown for clarity. (A; left) Open$_{Ms}$ (pale green) and (middle) pOpen$_{Ms}$ (turquoise) structures. (B; middle) Closed$_{Ab}$ (slate) and overlay (right) comparison of Closed$_{Ab}$ and Open$_{Ms}$. (C) As in B for Inactivated$_{Ab}$ (AB tetramer; gray). (D) As in B for Inactivated$_{Ab}$ (CD tetramer; gray). (E) As in B for Closed$_{Ae}$ (raspberry). The distances between the narrowest parts of the SFs in each case are given in Table S1.

ends of their S6 helices away from the pore axis. Also, the N-terminal ends of the S5 helices appear to have moved slightly with respect to each other. Had the open pore structure had its VS attached, this latter movement would have impinged on the S4–S5 linker (Fig. 3 A, circle) of an adjacent monomer. We speculate that the reason the NavAb pore is closed is that the linker region is in the closed conformation, and that if the linker had been more closely coupled to the VS in its open conformation in the crystal, the NavAb pore structure would also have been of an open conformation.

When the structures of the S6 pore helices of all the conformations are examined in detail (Fig. 3 B), the differences at the quaternary structural level between the open and closed (and inactivated) structures appear to arise from a twist in the middle of the S6 helix structures beginning at residue T206. The extracellular ends of all of the S6 helices in all of the closed and inactivated structures superimpose closely (Fig. 3 B), but the $Open_{Ms}$ structure is an outlier. This results from a change in the backbone Ramachandran angles between the open and closed forms, which perpetrates along the C-terminal end of S6 starting at T206 (Fig. 3 C). The consequence of this deviation is that the C-terminal end of the S6 helix in the $Open_{Ms}$ structure moves away from the axis of the top part of the helix, thereby opening the activation gate. In the lower resolution $pOpen_{Ms}$ structure, residue T209 appeared to be the focal point of the bend, but in the higher resolution fully $Open_{Ms}$ structure, it is clear that the beginning of the bend occurs one turn earlier in S6, at T206. Notably, the changes between open and closed structures are subtle enough so that they do not change the secondary structure (Fig. 3 D) of the S6 helix. What starts as a relatively small change in the middle of the helix is translated to a motion of >5 Å at the end of S6 that forms the activation gate. This suggests a simple (energetically inexpensive) mechanism for opening and closing: a twist in the backbone that does not disrupt the hydrogen bonding pattern is sufficient to open the gate. It does not require major rearrangements of the rest of the structure and is thus compatible with a rapid opening, such as that which gives rise to the initial phase of the action potential in excitable cells. The asynchrony of the motions of the four monomers, as suggested by the partially open structure, suggests that there may also be an asynchrony of the process of opening.

The open and closed structures have very similar cavity regions (Fig. 2 A), with a minor hydrophobic constriction (designated HC1) near the bottom of the cavity (Fig. 2 A) near residue I215 in NavMs (equivalent to V213 in NavAb) that is not sufficient to prevent ions continuing their passage. However, the $Closed_{Ab}$ form has two additional major hydrophobic constrictions (HC2 and HC3) further down toward the extracellular surface (Fig. 2 A) at approximately the level of residues M221 and I217 (numbering according to NavAb sequence; notably, the latter corresponds to the site of the mutation to a cysteine in the NavAb construct). Neither of these constrictions is seen in the open NavMs structure. HC3 (which obscures the exit) would exclude passage of even totally dehydrated sodium ions in the closed structure.

Because the SFs of NavMs and NavAb have identical sequences (TLESWS; Fig. 1), they can be directly compared. The SFs of the $Open_{Ms}$ (Fig. 4 A) and $Closed_{Ab}$ (Fig. 4 B) structures are superimposable (Fig. 4 B, right), thus indicating that the closing of the activation gate, which prevents ion translocation, does not affect the potential entry of ions into the pore. In contrast, the SFs of the inactivated forms (Fig. 4, C and D) are very different from those of both the open and closed states, suggesting that they are altered during the inactivation process.

The structure and role of the CTD in opening and closing

All of the initial crystal structures determined (NavAb, NavMs, and NavRh) have elucidated the nature of the transmembrane domains (effectively to the end of the S6 helix) of the channels, but the structures of their CTDs (beyond the end of helix S6) were not interpretable, although these regions were present in the proteins used to produce the crystals. The structure of the CTD of the open conformation was first determined not by crystallography but by a combination of spectroscopic methods (Powl et al., 2010; Bagnéris et al., 2013), and shown to have a disordered region adjacent to the activation gate and a distal coiled-coil region (Figs. 1 and 5); molecular dynamics calculations (Bagnéris et al., 2013) suggested that flexibility of the region adjacent to the activation gate in the open state could account for the lack of defined structure in the crystal. The CTD in the closed NavAe pore (Shaya et al., 2014) is the only other such domain that has been defined structurally, this time by crystallographic means. Like the open CTD, its distal end formed a coiled-coil, but unlike the open CTD, the proximal end of the structure, nearest to the activation gate, was helical and relatively well ordered. These observations suggested that although the C-terminal end of the CTD remains unchanged in the two states, the end adjacent to the activation gate undergoes an ordered-to-disordered transition when the gate is opened (Fig. 5), thereby accommodating the separation movement at the end of the S6 helix that forms the gate, without uncoiling the distal coiled-coil that has been proposed to have a structural role in stabilizing the tetrameric structure in the membrane (Mio et al., 2010; Powl et al., 2010). Functional studies on the NavMs channel (Bagnéris et al., 2013), as well as on another orthologue (NavSulP from *Sulfitobacer pontiacus*; Irie et al., 2012), have indicated that this region (especially the EEE motif near the top of the CTD) plays a role in inactivation, recovery, and closing, perhaps by promotion of the conformational change of the S6 helix. In

addition, in the NavAe pore structure, there is some density in the extracellular region beyond the end of the transmembrane segments that could be a calcium or other cation. Domain DIV of the human Nav1.4 sodium channel also possesses a similar negatively charged region just after its activation gate (Fig. 1), which appears to be a common feature in the prokaryotic sodium channels.

What produces the open and closed states in the crystals?

An obvious suggestion as to what causes NavMs pore structure to be open is that it is missing the constraints provided by the VS and S4–S5 linker regions present in the full-length channel structures. However, this cannot be the only reason, as the two structures of pore-only constructs, NavMs and NavAe, are in different states (NavMs is open, whereas NavAe is closed). It is also not because of the presence of CTD structures because, again, the CTDs are present in both of these two structures, albeit in different conformations. Furthermore, the partially open NavMs construct is missing the distal end of its CTD, yet one of its monomers is in the open state. The CTDs are present but not visible in any of the other structures. It is possible that the different CTD structures have a role in driving the transition (for example because of the different conformations at their N-terminal ends), but this cannot be determined from the structures in hand. It could also be because of the differences in crystal packing that enable the NavMs pores to open: in the NavMs crystals, the transmembrane regions of different pores are aligned next to each other, as if in a membrane bilayer, with a large enough gap to fit the CTD between two separate bilayers and thus allow sufficient room for the bottom of the pore to open. In the NavAe crystals, the CTDs are sandwiched between other CTDs and pore regions of symmetrically

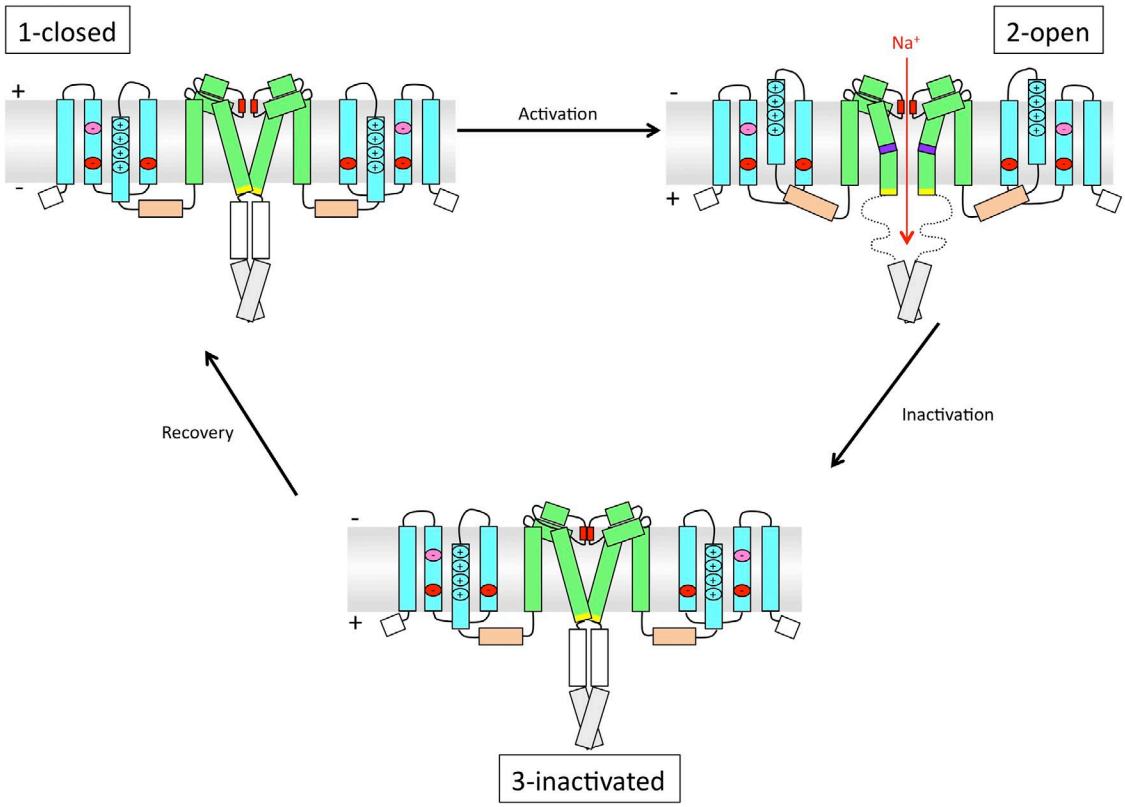

Figure 5. Schematic diagram of (1) closed, (2) open, and (3) inactivated states of prokaryotic sodium channels based on crystallographic studies. Only two monomers are shown in each figure for clarity. The color scheme is as in Fig. 1. The VS S1–S4 helices are depicted as cyan bars, the S4–S5 linker is an orange bar, the S5–S6 helices of the pore region are green bars, and the coiled-coil region of the CTD is gray. The extracellular negatively charged region in S2 is in a magenta circle, and the intracellular negatively charged regions in S2 and S3 are in red circles. The four arginines in S4 involved in the gating charge transfer across the membrane through sequential interactions, with the extracellular negatively charged region and the intracellular negatively charged region represented by a "+." The residues forming the SF are indicated by red boxes. The residue in purple is the start of the S6 twist that results in the open gate; the residue in yellow is the third hydrophobic constriction site in the closed form, which is not constricted in the open form, and indicates the position of the activation gate. The white bars represent the helical region present in the CTD in the closed and inactivated structures, and the corresponding dotted gray lines are the disordered CTD linker region in the open conformation.

related molecules, rigidifying the whole structure and potentially preventing the opening.

The different structures in the crystals may be caused by (or alternatively, result in) the presence or absences of ions within the pore, as sodium ions are visible in the SF of only the NavMs open-state crystal forms. However, in a version of the NavAb orthologue engineered to be calcium selective (Tang et al., 2014), the presence of calcium ions in that pore did not produce an open state, so the mere presence of ions appears not to be sufficient to produce an open pore. The most likely candidate in vivo is the VS-pore linker between helices S4 and S5, which could act as a lever, either pushing or pulling the pore domain when the VS is activated to its "up" position. But the linker is not present in either the NavMs open or partially open structures, nor in the NavAe closed structures. And although it is present in the NavAb structures, it is in the "wrong" position to influence the opening of the pore, so it may be a contributing, but not the only, driving force. This is an important issue and will need to be resolved in the future to enable a full understanding of the opening and closing processes.

Structural transitions associated with inactivation

Comparisons of the structure of the $Inactivated_{Ab}$ channel with both the $Closed_{Ab}$ and $Open_{Ms}$ structures indicate areas of the protein primarily involved in the inactivation transition. The $Inactivated_{Ab}$ structure has a very similar upper cavity region to both the open and closed structures, and an asymmetric inactivation gate conformation that, like the symmetrical gate of the closed state, is occluded. The activation gate structures of the S6 helices of both the $Inactivated_{Ab}$ and $Inactivated_{Rh}$ channels closely overlay the $Closed_{Ab}$ (Fig. 3 B) but not the $Open_{Ms}$ structures, suggesting that the hinge necessary to open the gate has not been activated. Although their S6 conformations appear to be the same, the structures of the two types of $Inactivated_{Ab}$ tetramers ("AB" and "CD") and the $Closed_{Ab}$ form do exhibit differences at their C-terminal ends: the inactivated forms have between two and eight fewer ordered residues visible in the crystals, suggesting that they exhibit more mobility or flexibility in this region. Because the CTD has not been resolved in any of the inactivated form crystals, we cannot make any conclusions about whether the regions adjacent to the transmembrane helices are disordered (as in the open state) or helical (as in the closed state). Nor can we discern even if they exhibit the same coiled-coil structures at their distal ends that are present in both the open and closed forms.

In contrast, the SF region of the $Inactivated_{Ab}$ structure (as well as that of the inactivated NavRh structure) is very different from either the open or closed states (Fig. 4). It has been described as "collapsed," and indeed it is of insufficient diameter to enable a full dehydrated sodium ion to enter into the pore, much less exit it. Because in this case comparisons can be made for two crystal structures of the same orthologue (NavAb), the differences in the inactivated and closed structures cannot be attributed to SF sequence differences. The changes involve both the P1 and P2 helices as well as the SF itself, and involve modest differences in the secondary structures of the turret and top of S5 (Fig. 3 D). The observation that structural changes associated with the inactivated structure primarily involve the SF region corresponds well with earlier functional studies suggesting that the region close to the SF is responsible for inactivation (Pavlov et al., 2005). Interestingly, too, is the correspondence with studies done many years ago using circular dichroism spectroscopy (Cronin et al., 2003) on eukaryotic (electric eel) sodium channels that were induced to adopt open, closed, and inactivated states through the use of toxins and drugs. Those functional studies indicated that the secondary structures of the open and closed channels were surprisingly very similar but that the secondary structures of the inactivated form was considerably different. This also corresponds with the structural observations for the prokaryotic channels, where there are no apparent changes in secondary structure between open and closed states but significant differences between the open and the inactivated state.

The structural comparisons thus suggest that inactivation closes not only the extracellular but also the intracellular ends of the transmembrane passageway, although the extracellular changes appear to be the defining ones for the inactivation state.

Structural models for sodium channel opening–closing–inactivation mechanisms

Early models (e.g., Armstrong and Bezanilla, 1973; Hille, 1975; Lehmann-Horn and Jurkat-Rott, 1999; see also Hille, 2001, and Armstrong, 2007) proposed for eukaryotic sodium channel charge movement and gating were based primarily on functional observations and were produced, for the most part, before either any sodium channel sequences were determined or any crystal structures of any members of the voltage-gated cation channel superfamily were available. Structural models included suggestions such as the constriction of the SF or the shutting of two flaps (Lehmann-Horn and Jurkat-Rott, 1999), one at the extracellular surface and one at the intracellular surface, as being responsible for inactivation and closing, respectively. With the sequencing of the first eukaryotic sodium channel (Noda et al., 1984), three-dimensional models were developed that proposed the involvement of specific regions for the activation and inactivation processes (Guy and Seetharamulu, 1986; Yu et al., 2005). Many other approaches, including mutational effects, interactions with toxins, drug and ligand binding, and various spectroscopic

studies, have since contributed to structure–function models of sodium channels (Catterall, 2012). More recently, the crystal structures of potassium channels (Doyle et al., 1998; Long et al., 2007) provided structural templates and information for understanding the electromechanical coupling and mechanism of their opening and closing. The sequence homology of sodium channels to these other members of the voltage-gated ion channel superfamily suggested that they would share a common architecture, albeit with very different SF regions, and led to more detailed models for sodium channel structures and functions (Yarov-Yarovoy et al., 2001; Shafrir et al., 2008; Zarrabi et al., 2010).

Soon after the prokaryotic sodium channels were identified as simpler target molecules for biophysical studies (Ren et al., 2001), and well before any of the prokaryotic orthologue crystal structures were determined, a hinge model for NaChBac (the first sodium channel orthologue whose sequence was determined) was proposed. This model for opening of the activation gate, like the models for the MthK potassium channel (Jiang et al., 2002), was based on the presence of a glycine residue in the middle of the S6 helix. Because glycines lack side chains, this type of residue could act as a flexible pivot for the top and bottom of the S6 helix, which could then move to open the gate. This model was supported by functional studies that showed that mutations of the glycine altered the rate of inactivation and recovery (Ito et al., 2004; Zhao et al., 2004), and spectroscopic studies that showed that changing the glycine to a conformationally less flexible serine produced a more thermally stable protein (O'Reilly et al., 2008); later molecular dynamics calculations (Barber et al., 2012) also supported a hinge-bending model involving this glycine. This model for the mechanism became less favored, however, after the determination of the sequences of other orthologues, as they did not have a glycine in the equivalent position.

The solution of the crystal structure of the prokaryotic sodium channel NavAb, with sequence and structural homology (especially in the VS regions) to single-domain tetrameric prokaryotic and eukaryotic potassium channel structures, prompted the suggestion (Payandeh et al., 2011) that the mechanism behind the coupling and pore opening might be similar to another model proposed for K^+ channels (Long et al., 2007). Indeed, the VS of the $Closed_{Ab}$ structure aligns well with the VS of the open Kv1.2 structure, although they diverge in the pore, specifically at the beginning of the base of the S5 helix, and their SFs are completely different both in sequence and in structure (one using side chains and backbone carbonyls, and the other narrower one using only backbone carbonyls to create the ion-binding sites). That model had the VS and pore regions moving as modular units, with the S4–S5 linker movement causing the conformational change. In the sodium channel case, the proposed change was a rotation-like motion of the S5 and S6 helices relative to each other, opening the pore in an iris-like dilation motion. This bears semblance to the twisting mechanism proposed for the opening and closing of the nonspecific ion channel in nicotinic acetylcholine receptors (Unwin, 2003), where the transmembrane helices of adjacent subunits change positions relative to each other, primarily on one surface, producing a rotational squeezing and release mechanism that changes the size of the pore along its length.

A new structure-based model for the opening–closing–inactivation mechanisms

The observed structural differences described above between $Open_{Ms}$ and $Closed_{Ab}$ do not support a model based on a modular S5–S6 iris-like motion. In the prokaryotic sodium channel crystal structures, the C-terminal end of the S5 helix exhibits very little change between the two different states, and nothing suggests its movement is coupled with that of the S6 helix in either the same or an adjacent subunit within the tetramer. Instead, the opening and closing appears to involve a twist/bend in the middle of the S6 helix, which moves the activation gate to occlude or open the intracellular surface, enabling ion egress from the cavity (McCusker et al., 2012; Bagnéris et al., 2013; Video 1). This is remarkably similar to the earlier hinge model, except that there is no glycine at the hinge position. Instead, a threonine (T206 in the NavMs numbering scheme) is located at the juncture, in an equivalent position in the sequence to the glycine found in the NaChBac orthologue. The structure of NavMs shows that there would be sufficient space to enable the backbone motion even with the threonine side chain, as the Cβ substituent does not impinge on the region that moves. However, the enhanced flexibility of a glycine residue in NaChBac could be responsible for its faster rate of opening (Ren et al., 2001) than NavMs (Ulmschneider et al., 2013).

Because the S1–S4 helices of the VS structure are already in the open conformation in the $Closed_{Ab}$ and $Inactivated_{Ab}$ structures, it initially seemed likely that the S4–S5 linker in these structures would be in a conformation similar to that which it would adopt in the open pore state. However, comparisons of the $Open_{Ms}$ and $Closed_{Ab}$ structures indicate that the positions of especially the S5 helices in the open pore would mitigate against the linker in the $Closed_{Ab}$ structure being completely in the activated state because the end of the open state S5 helix would impinge on the linker. It is therefore suggested that the linker is in a "primed" state but that it moves in concert with the S5 and S6 helices as the activation gate is opened.

The structure-based model for the slow inactivation process, like several of the early models (Lehmann-Horn and Jurkat-Rott, 1999), appears to primarily involve a closing of the SF to ion entry on the extracellular surface

(Fig. 5). Rather than a flap folding over the entry, however, it appears that the SF itself folds in toward the center of the ion pathway, blocking entry of any sodium ions into the pore. It also appears, contrary to the double-flap mechanism, that the activation gate in the inactivated form is closed rather than open, although this could be a consequence of the crystallization and packing conditions (Video 2).

Flexibility at the C-terminal region of S6 thus appears to be the defining feature of the prokaryotic voltage-gated sodium channel. It may be at least partially responsible for channel opening and for the cascade of events that occur at the SF and P loops during inactivation. The presence of a flexible linking region to the CTD would enable the opening and closing to occur without uncoiling the distal coiled-coil region, which may play an important role in stabilizing the tetrameric quaternary structure of the prokaryotic sodium channels (Video 3). This feature is not present (nor necessary) in eukaryotic sodium channels, which are single polypeptide chains. Instead, they seem to have a CTD that plays an important role in fast inactivation, a function that prokaryotic sodium channels do not exhibit.

Similarities and differences in the activation mechanisms of prokaryotic and eukaryotic sodium channels

Prokaryotic and eukaryotic sodium channels exhibit considerable homologies in the sequences of their transmembrane regions (Fig. 1), especially in the C-terminal ends of their S6 helices, although their SFs and CTDs are entirely different. Likewise, both exhibit transitions between activation, recovery, and slow inactivation functional states, albeit with different kinetics (as well as the absence of fast inactivation in prokaryotic channels). Therefore, it is of interest to consider if they might involve similar structural features in a common mechanism for opening and closing.

New studies (Bagnéris et al., 2014) on the structure and electrophysiological consequences of binding channel blocker drugs to prokaryotic and human $Na_v1.1$ channels have shown the parallel nature of their block by a range of ligands that bind in the hydrophobic cavity and prevent passage of ions from the extracellular to intracellular surfaces. This apparently occurs not by closing the activation gate but by the hydrophobic ligands creating a barrier to exit at the end of the SF region, and is entirely consistent with the mechanisms described above.

Furthermore, a recent study was done to test whether a similar mechanism of opening and closing could be operating in human Nav1.4 and prokaryotic sodium channels (Oelstrom et al., 2014). Channels with their fast inactivation mechanism disabled could be functionally held in either the open or closed state. An accessibility labeling technique was used to probe sites in S6 of domain IV (Fig. 1). Residues C terminal to the proposed activation gate were accessible to labeling from the intracellular side in both the open and closed states, whereas residues above this were only accessible in the open state. In the open state, the channel could be labeled up to the ring of hydrophobic residues immediately preceding the equivalent to residue T206 in the prokaryotic channels, again consistent with a mechanism involving a hinge mechanism in the middle of S6. These results strongly support the type of mechanism for opening and closing presented above, with a flexible hinge region that opens the pore up to the intracellular compartment in the open state, but not in the closed state.

However, it is important to note that significant differences in the activation/inactivation and selectivity mechanisms do exist between prokaryotic and eukaryotic channels (see, for example, Ahern, 2013; Goldschen-Ohm et al., 2013; Finol-Urdaneta et al., 2014, for detailed discussions). These arise in large part because of the asymmetry of the pseudotetrameric eukaryotic structures as opposed to the simpler homotetramers that comprise the prokaryotic channels. They result in asynchronous movements of VSs, asymmetric ion-binding sites, and novel loops between the different domains that have specialized roles, for example in fast inactivation, which are not seen in the prokaryotic channels. Nevertheless, the availability of several crystal forms of prokaryotic voltage-gated sodium channels in different conformational states has vastly increased our knowledge of the structure–function relationships for these channels, and provides new insight into their mechanisms of opening, closing, and inactivation (Fig. 5). These, in turn, may inform our understanding of both the structure and function of sodium channels in general. The new model proposed, based on the detailed structures of prokaryotic channels in crystal environments, will, however, await confirmation by further functional experiments on channels in their biological context, as well as structural studies of eukaryotic channels.

This work was supported by grants from the UK Biotechnology and Biological Sciences Research Council (to B.A. Wallace).

The authors declare no competing financial interests.

Elizabeth M. Adler served as editor.

Submitted: 11 June 2014
Accepted: 10 November 2014

REFERENCES

Ahern, C.A. 2013. What activates inactivation? *J. Gen. Physiol.* 142:97–100. http://dx.doi.org/10.1085/jgp.201311046

Armstrong, C.M. 2007. Life among the axons. *Annu. Rev. Physiol.* 69:1–18. http://dx.doi.org/10.1146/annurev.physiol.69.120205.124448

Armstrong, C.M., and F. Bezanilla. 1973. Currents related to movement of the gating particles of the sodium channels. *Nature.* 242:459–461. http://dx.doi.org/10.1038/242459a0

Bagnéris, C., P.G. DeCaen, B.A. Hall, C.E. Naylor, D.E. Clapham, C.W.M. Kay, and B.A. Wallace. 2013. Role of the C-terminal domain in the structure and function of tetrameric sodium channels. *Nat. Commun.* 4:2465. http://dx.doi.org/10.1038/ncomms3465

Bagnéris, C., P.G. DeCaen, C.E. Naylor, D.C. Pryde, I. Nobeli, D.E. Clapham, and B.A. Wallace. 2014. Prokaryotic NavMs channel as a structural and functional model for eukaryotic sodium channel antagonism. *Proc. Natl. Acad. Sci. USA.* 111:8428–8433. http://dx.doi.org/10.1073/pnas.1406855111

Barber, A.F., V. Carnevale, S.G. Raju, C. Amaral, W. Treptow, and M.L. Klein. 2012. Hinge-bending motions in the pore domain of a bacterial voltage-gated sodium channel. *Biochim. Biophys. Acta.* 1818: 2120–2125. http://dx.doi.org/10.1016/j.bbamem.2012.05.002

Catterall, W.A. 2012. Voltage-gated sodium channels at 60: structure, function and pathophysiology. *J. Physiol.* 590:2577–2589. http://dx.doi.org/10.1113/jphysiol.2011.224204

Charalambous, K., and B.A. Wallace. 2011. NaChBac: The long lost sodium channel ancestor. *Biochemistry.* 50:6742–6752. http://dx.doi.org/10.1021/bi200942y

Chovancova, E., A. Pavelka, P. Benes, O. Strnad, J. Brezovsky, B. Kozlikova, A. Gora, V. Sustr, M. Klvana, P. Medek, et al. 2012. CAVER 3.0: A tool for the analysis of transport pathways in dynamic protein structures. *PLOS Comput. Biol.* 8:e1002708. http://dx.doi.org/10.1371/journal.pcbi.1002708

Cronin, N.B., A. O'Reilly, H. Duclohier, and B.A. Wallace. 2003. Binding of the anticonvulsant drug lamotrigine and the neurotoxin batrachotoxin to voltage-gated sodium channels induces conformational changes associated with block and steady-state activation. *J. Biol. Chem.* 278:10675–10682. http://dx.doi.org/10.1074/jbc.M208356200

D'Avanzo, N., E.C. McCusker, A.M. Powl, A.J. Miles, C.G. Nichols, and B.A. Wallace. 2013. Differential lipid dependence of the function of bacterial sodium channels. *PLoS ONE.* 8:e61216. http://dx.doi.org/10.1371/journal.pone.0061216

DeCaen, P.G., V. Yarov-Yarovoy, Y. Zhao, T. Scheuer, and W.A. Catterall. 2008. Disulfide locking a sodium channel voltage sensor reveals ion pair formation during activation. *Proc. Natl. Acad. Sci. USA.* 105:15142–15147. http://dx.doi.org/10.1073/pnas.0806486105

DeCaen, P.G., V. Yarov-Yarovoy, E.M. Sharp, T. Scheuer, and W.A. Catterall. 2009. Sequential formation of ion pairs during activation of a sodium channel voltage sensor. *Proc. Natl. Acad. Sci. USA.* 106:22498–22503. http://dx.doi.org/10.1073/pnas.0912307106

Doyle, D.A., J. Morais Cabral, R.A. Pfeutzner, A. Kuo, J.M. Gulbis, S.L. Cohen, B.T. Chait, and R. MacKinnon. 1998. The structure of the potassium channel: Molecular basis of K^+ conduction and selectivity. *Science.* 280:69–77. http://dx.doi.org/10.1126/science.280.5360.69

Finol-Urdaneta, R.K., Y. Wang, A. Al-Sabi, C. Zhao, S.Y. Noskov, and R.J. French. 2014. Sodium channel selectivity and conduction: Prokaryotes have devised their own molecular strategy. *J. Gen. Physiol.* 143:157–171. http://dx.doi.org/10.1085/jgp.201311037

Goldschen-Ohm, M.P., D.L. Capes, K.M. Oelstrom, and B. Chanda. 2013. Multiple pore conformations driven by asynchronous movements of voltage sensors in a eukaryotic sodium channel. *Nat. Commun.* 4:1350. http://dx.doi.org/10.1038/ncomms2356

Guy, H.R., and P. Seetharamulu. 1986. Molecular model of the action potential sodium channel. *Proc. Natl. Acad. Sci. USA.* 83:508–512. http://dx.doi.org/10.1073/pnas.83.2.508

Hille, B. 1975. Ionic selectivity, saturation, and block in sodium channels. A four-barrier model. *J. Gen. Physiol.* 66:535–560. http://dx.doi.org/10.1085/jgp.66.5.535

Hille, B. 2001. Ion Channels of Excitable Membranes. Sinauer Associates, Sunderland, MA. 814 pp.

Irie, K., T. Shimomura, and Y. Fujiyoshi. 2012. The C-terminal helical bundle of the tetrameric prokaryotic sodium channel accelerates the inactivation rate. *Nat. Commun.* 3:793. http://dx.doi.org/10.1038/ncomms1797

Ito, M., H. Xu, A.A. Guffanti, Y. Wei, L. Zvi, D.E. Clapham, and T.A. Krulwich. 2004. The voltage-gated Na^+ channel Na_VBP has a role in motility, chemotaxis, and pH homeostasis of an alkaliphilic *Bacillus*. *Proc. Natl. Acad. Sci. USA.* 101:10566–10571. http://dx.doi.org/10.1073/pnas.0402692101

Jiang, Y., A. Lee, J. Chen, M. Cadene, B.T. Chait, and R. MacKinnon. 2002. The open pore conformation of potassium channels. *Nature.* 417:523–526. http://dx.doi.org/10.1038/417523a

Klose, D.P., B.A. Wallace, and R.W. Janes. 2010. 2Struc: the secondary structure server. *Bioinformatics.* 26:2624–2625. http://dx.doi.org/10.1093/bioinformatics/btq480

Koishi, R., H. Xu, D. Ren, B. Navarro, B.W. Spiller, Q. Shi, and D.E. Clapham. 2004. A superfamily of voltage-gated sodium channels in bacteria. *J. Biol. Chem.* 279:9532–9538. http://dx.doi.org/10.1074/jbc.M313100200

Kuzmenkin, A., F. Bezanilla, and A.M. Correa. 2004. Gating of the bacterial sodium channel, NaChBac: Voltage-dependent charge movement and gating currents. *J. Gen. Physiol.* 124:349–356. http://dx.doi.org/10.1085/jgp.200409139

Lehmann-Horn, F., and K. Jurkat-Rott. 1999. Voltage-gated ion channels and hereditary disease. *Physiol. Rev.* 79:1317–1372.

Long, S.B., X. Tao, E.B. Campbell, and R. MacKinnon. 2007. Atomic structure of a voltage-dependent K^+ channel in a lipid membrane-like environment. *Nature.* 450:376–382. http://dx.doi.org/10.1038/nature06265

McCusker, E.C., N. D'Avanzo, C.G. Nichols, and B.A. Wallace. 2011. Simplified bacterial "pore" channel provides insight into the assembly, stability, and structure of sodium channels. *J. Biol. Chem.* 286:16386–16391. http://dx.doi.org/10.1074/jbc.C111.228122

McCusker, E.C., C. Bagnéris, C.E. Naylor, A.R. Cole, N. D'Avanzo, C.G. Nichols, and B.A. Wallace. 2012. Structure of a bacterial voltage-gated sodium channel pore reveals mechanisms of opening and closing. *Nat. Commun.* 3:1102. http://dx.doi.org/10.1038/ncomms2077

Mio, K., M. Mio, F. Arisaka, M. Sato, and C. Sato. 2010. The C-terminal coiled-coil of the bacterial voltage-gated sodium channel NaChBac is not essential for tetramer formation, but stabilizes subunit-to-subunit interactions. *Prog. Biophys. Mol. Biol.* 103:111–121. http://dx.doi.org/10.1016/j.pbiomolbio.2010.05.002

Noda, M., S. Shimizu, T. Tanabe, T. Takai, T. Kayano, T. Ikeda, H. Takahashi, H. Nakayama, Y. Kanaoka, N. Minamino, et al. 1984. Primary structure of *Electrophorus electricus* sodium channel deduced from cDNA sequence. *Nature.* 312:121–127. http://dx.doi.org/10.1038/312121a0

Nurani, G., M. Radford, K. Charalambous, A.O. O'Reilly, N.B. Cronin, S. Haque, and B.A. Wallace. 2008. Tetrameric bacterial sodium channels: Characterization of structure, stability, and drug binding. *Biochemistry.* 47:8114–8121. http://dx.doi.org/10.1021/bi800645w

O'Reilly, A.O., K. Charalambous, G. Nurani, A.M. Powl, and B.A. Wallace. 2008. G219S mutagenesis as a means of stabilizing conformational flexibility in the bacterial sodium channel NaChBac. *Mol. Membr. Biol.* 25:670–676. http://dx.doi.org/10.1080/09687680802508754

Oelstrom, K., M.P. Goldschen-Ohm, M. Holmgren, and B. Chanda. 2014. Evolutionarily conserved intracellular gate of voltage-dependent sodium channels. *Nat. Commun.* 5:3420. http://dx.doi.org/10.1038/ncomms4420

Pavlov, E., C. Bladen, R. Winkfein, C. Diao, P. Dhaliwal, and R.J. French. 2005. The pore, not cytoplasmic domains, underlies inactivation in a prokaryotic sodium channel. *Biophys. J.* 89:232–242. http://dx.doi.org/10.1529/biophysj.104.056994

Payandeh, J., T. Scheuer, N. Zheng, and W.A. Catterall. 2011. The crystal structure of a voltage-gated sodium channel. *Nature.* 475:353–358. http://dx.doi.org/10.1038/nature10238

Payandeh, J., T.M. Gamal El-Din, T. Scheuer, N. Zheng, and W.A. Catterall. 2012. Crystal structure of a voltage-gated sodium channel in two potentially inactivated states. *Nature.* 486:135–139.

Powl, A.M., A.O. O'Reilly, A.J. Miles, and B.A. Wallace. 2010. Synchrotron radiation circular dichroism spectroscopy-defined structure of the C-terminal domain of NaChBac and its role in channel assembly. *Proc. Natl. Acad. Sci. USA.* 107:14064–14069. http://dx.doi.org/10.1073/pnas.1001793107

Ren, D., B. Navarro, H. Xu, L. Yue, Q. Shi, and D.E. Clapham. 2001. A prokaryotic voltage-gated sodium channel. *Science.* 294:2372–2375. http://dx.doi.org/10.1126/science.1065635

Shafrir, Y., S.R. Durell, and H.R. Guy. 2008. Models of voltage-dependent conformational changes in NaChBac channels. *Biophys. J.* 95:3663–3676. http://dx.doi.org/10.1529/biophysj.108.135335

Shaya, D., M. Kreir, R.A. Robbins, S. Wong, J. Hammon, A. Brüggemann, and D.L. Minor Jr. 2011. Voltage-gated sodium channel (NaV) protein dissection creates a set of functional pore-only proteins. *Proc. Natl. Acad. Sci. USA.* 108:12313–12318. http://dx.doi.org/10.1073/pnas.1106811108

Shaya, D., F. Findeisen, F. Abderemane-Ali, C. Arrigoni, S. Wong, S.R. Nurva, G. Loussouarn, and D.L. Minor Jr. 2014. Structure of a prokaryotic sodium channel pore reveals essential gating elements and an outer ion binding site common to eukaryotic channels. *J. Mol. Biol.* 426:467–483. http://dx.doi.org/10.1016/j.jmb.2013.10.010

Sievers, F., A. Wilm, D. Dineen, T.J. Gibson, K. Karplus, W. Li, R. Lopez, H. McWilliam, M. Remmert, J. Söding, et al. 2011. Fast, scalable generation of high-quality protein multiple sequence alignments using Clustal Omega. *Mol. Syst. Biol.* 7:539. http://dx.doi.org/10.1038/msb.2011.75

Tang, L., T.M. Gamal El-Din, J. Payandeh, G.Q. Martinez, T.M. Heard, T. Scheuer, N. Zheng, and W.A. Catterall. 2014. Structural basis for Ca^{2+} selectivity of a voltage-gated calcium channel. *Nature.* 505:56–61. http://dx.doi.org/10.1038/nature12775

Tsai, C.-J., K. Tani, K. Irie, Y. Hiroaki, T. Shimomura, D.G. McMillan, G.M. Cook, G.F.X. Schertler, Y. Fujiyoshi, and X.-D. Li. 2013. Two alternative conformations of a voltage-gated sodium channel. *J. Mol. Biol.* 425:4074–4088. http://dx.doi.org/10.1016/j.jmb.2013.06.036

Ulmschneider, M.B., C. Bagnéris, E.C. McCusker, P.G. DeCaen, M. Delling, D.E. Clapham, J.P. Ulmschneider, and B.A. Wallace. 2013. Molecular dynamics of ion transport through the open conformation of a bacterial voltage-gated sodium channel. *Proc. Natl. Acad. Sci. USA.* 110:6364–6369. http://dx.doi.org/10.1073/pnas.1214667110

Unwin, N. 2003. Structure and action of the nicotinic acetylcholine receptor explored by electron microscopy. *FEBS Lett.* 555:91–95. http://dx.doi.org/10.1016/S0014-5793(03)01084-6

Yarov-Yarovoy, V., J. Brown, E.M. Sharp, J.J. Clare, T. Scheuer, and W.A. Catterall. 2001. Molecular determinants of voltage-dependent gating and binding of pore-blocking drugs in transmembrane segment IIIS6 of the Na^+ channel alpha subunit. *J. Biol. Chem.* 276:20–27. http://dx.doi.org/10.1074/jbc.M006992200

Yu, F.H., V. Yarov-Yarovoy, G.A. Gutman, and W.A. Catterall. 2005. Overview of molecular relationships in the voltage-gated ion channel superfamily. *Pharmacol. Rev.* 57:387–395. http://dx.doi.org/10.1124/pr.57.4.13

Zarrabi, T., R. Cervenka, W. Sandtner, P. Lukacs, X. Koenig, K. Hilber, M. Mille, G.M. Lipkind, H.A. Fozzard, and H. Todt. 2010. A molecular switch between the outer and the inner vestibules of the voltage-gated Na^+ channel. *J. Biol. Chem.* 285:39458–39470. http://dx.doi.org/10.1074/jbc.M110.132886

Zhang, X., W. Ren, P. DeCaen, C. Yan, X. Tao, L. Tang, J. Wang, K. Hasegawa, T. Kumasaka, J. He, et al. 2012. Crystal structure of an orthologue of the NaChBac voltage-gated sodium channel. *Nature.* 486:130–134.

Zhao, Y., V. Yarov-Yarovoy, T. Scheuer, and W.A. Catterall. 2004. A gating hinge in Na^+ channels: A molecular switch for electrical signaling. *Neuron.* 41:859–865. http://dx.doi.org/10.1016/S0896-6273(04)00116-3